Bioelectrochemistry 111 (2016) 93–99

Contents lists available at ScienceDirect

Bioelectrochemistry

journal homepage: www.elsevier.com/locate/bioelechem

Electrocatalytic processes promoted by diamond nanoparticles in enzymatic biosensing devices

M. Briones [a], M.D. Petit-Domínguez [a], A.M. Parra-Alfambra [a], L. Vázquez [c], F. Pariente [a], E. Lorenzo [a,b], E. Casero [a,*]

[a] Departamento de Química Analítica y Análisis Instrumental, Facultad de Ciencias, c/ Francisco Tomás y Valiente, N°7, Campus de Excelencia de la Universidad Autónoma de Madrid, 28049 Madrid, Spain
[b] Instituto Madrileño de Estudios Avanzados (IMDEA) - Nanoscience, Faraday 9, Campus Cantoblanco-UAM, 28049 Madrid, Spain
[c] Instituto de Ciencia de Materiales de Madrid (CSIC), c/ Sor Juana Inés de la Cruz N°3, Campus de Excelencia de la Universidad Autónoma de Madrid, 28049 Madrid, Spain

ARTICLE INFO

Article history:
Received 3 December 2015
Received in revised form 23 May 2016
Accepted 24 May 2016
Available online 26 May 2016

Keywords:
Diamond nanoparticles
Electrochemical biosensors
Lactate determination
(Hydroxymethyl)ferrocene

ABSTRACT

We have developed a biosensing platform for lactate determination based on gold electrodes modified with diamond nanoparticles of 4 nm of nominal diameter, employing the enzyme lactate oxidase and (hydroxymethyl)ferrocene (HMF) as redox mediator in solution. This system displays a response towards lactate that is completely different to those typically observed for lactate biosensors based on other nanomaterials, such as graphene, carbon nanotubes, gold nanoparticles or even diamond nanoparticles of greater size. We have observed by cyclic voltammetry that, under certain experimental conditions, an irreversible wave ($E^0 = +0.15$ V) appears concomitantly with the typical Fe^{II}/Fe^{III} peaks ($E^0 = +0.30$ V) of HMF. In this case, the biosensor response to lactate shows simultaneous electrocatalytic peaks at +0.15 V and +0.30 V, indicating the concurrence of different feedback mechanisms. The achievement of a biosensor response to lactate at +0.15 V is very convenient in order to avoid potential interferences. The developed biosensor presents a linear concentration range from 0.02 mM to 1.2 mM, a sensitivity of 6.1 μA mM^{-1}, a detection limit of 5.3 μM and excellent stability. These analytical properties compare well with those obtained for other lactate-based biosensors that also include nanomaterials and employ HMF as redox mediator.

1. Introduction

Nowadays, the employment of different kinds of nanomaterials, such as metallic nanoparticles, carbon nanotubes or graphene, in the development of electrochemical biosensors is a field of great interest [1,2]. These nanomaterials present important characteristics that contribute to increase the performance of the biosensing devices. Among them, it can be highlighted a large specific surface area, a high electronic conductivity and an increase in the surface functionalization possibilities. From the point of view of electrochemical biosensing, these nanomaterials offer not only a large surface area for immobilizing a high amount of a wide variety of recognition biomolecules, but also promote the electron transfer between the electrode surface and the biomolecule [3].

Recently, a member of the carbon nanomaterials family, denoted as diamond nanoparticles (DNPs), has also become a promising alternative for biosensor development. Until now, although they present a wide range of interesting properties, DNPs have been less employed for this purpose than the rest of the carbon nanomaterials. Among the properties that make them suitable candidates for biosensing can be mentioned [4–7]: i) their production at large-scale by detonation methods with a narrow size distribution and a moderate cost, ii) the presence on their surface, as a consequence of the production and purification methods, of several oxygenated functional groups, which facilitate the immobilization of biomolecules (peptide nucleic acids, antibodies, enzymes) [8–11] and iii) their biocompatibility and noncytotoxic nature.

In contrast to these excellent properties, diamond material has an insulating character, with a band gap of 5.47 eV [12], which is, in principle, inadequate for electrochemical applications. However, several fundamental studies have shown that, despite the great bandgap value, electrodes modified with DNPs exhibit a high electrochemical response towards different charged redox probes in solution such as $Fe(CN_6)^{3-/4-}$, $Ru(NH_3)_6^{2+/3+}$, $Ru(CN)_6^{3-/4-}$, $IrCl_6^{2-/3-}$ [13–15], and they are also able to promote direct electron transfer between redox enzymes and the underlying electrode [16]. This unexpected behavior is due to the existence of discrete electronic states within the diamond band gap originated by the overlapping of molecular orbitals of the different functionalities with unsaturated bonding present on the diamond nanoparticles surface. Therefore, DNPs can be either oxidized or reduced depending on their potential relative to the underlying electrode or to a redox probe [13,14]. Recently, the electrochemical behavior of neutral redox probes in solution has also been studied

* Corresponding author.
E-mail address: elena.casero@uam.es (E. Casero).

http://dx.doi.org/10.1016/j.bioelechem.2016.05.007
1567-5394/

employing DNPs modified electrodes, showing an oxidation/reduction current even higher than that obtained for charged species [17].

However, the employment of DNPs in biosensors development is still scarce. In this sense, in a previous work, we reported [18] the development of an electrochemical enzymatic biosensor nanostructured with diamond nanoparticles of 9 nm of nominal diameter (DNPs9), employing a neutral probe, (hydroxymethyl)ferrocene, as redox mediator in solution. The results obtained demonstrated the suitability of this nanomaterial to prepare high performance electrochemical biosensing platforms that allow lactate determination at +0.30 V. In the present work, we want to go one step further by developing a similar biosensing platform, but based on DNPs of smaller size (4 nm of nominal diameter), that allows diminishing the potential value for lactate determination. To undertake this study, we started delving into the effect of several factors, such as pH and scan rate on the HMF electrochemical behavior at 4 nm DNPs modified gold electrodes (DNPs4/Au). Once these parameters were optimized, lactate oxidase (LOx) was immobilized onto the DNPs4 modified electrode and the electrocatalytic response of the LOx/DNPs4/Au system towards lactate was studied and compared with those of the LOx/DNPs9/Au biosensor. Finally, a similar biosensor, but based on glucose oxidase, was fabricated in order to assess the broad applicability of the developed platform.

2. Experimental section

2.1. Materials

Diamond nanoparticles (DNPs4 and DNPs9) are obtained from SkySpring Nanomaterials (Products 0510HZ and 0512HZ, respectively), Inc. (Houston, TX). According to data provided by the manufacturer, DNPs contain —OH, —CN, —COOH, C—O—C and C═O as functionality groups and their nominal diameters are 3–4 nm and 4–15 nm, respectively. DNPs suspensions (1 mg mL^{-1}) were prepared in water. Lactate oxidase (LOx, EC 232-841-6 from *Pediococcus* species) and glucose oxidase (GOx, EC 1.1.3.4 from *Aspergillus niger*) lyophilized powder containing 41 units/mg solid and 15,200 units/g solid, respectively were obtained from the Sigma Chemical Co. (St. Louis, MO). Stock solutions were prepared dissolving 1.3 mg of the LOx lyophilized powder in 500 μL of 0.1 M phosphate buffer solution (pH = 7.0) and 7.5 mg of the GOx lyophilized powder in 250 μL of 0.1 M phosphate buffer solution (pH = 7.0). The enzyme solutions were aliquoted (10 μL) and stored at −30 °C. Under these conditions, the enzymatic activity remains stable for several weeks. L-(+)-Lactic acid lithium salt 97%, D-(+)-glucose (99.5%) and (hydroxymethyl)ferrocene (HMF) were obtained from Aldrich Chemical Co. (Milwaukee, WI). An enzymatic assay kit for lactate determination (K-LATE 07/14) was purchased from Megazyme (Ireland). Sodium phosphate (Merck) was employed for the preparation of buffer solutions. Other chemicals used in this work were reagent grade quality and used as received without additional purification steps. Water was purified with a Millipore Milli-Q-System. All solutions were prepared just prior to use.

2.2. Experimental techniques

Electrochemical measurements were carried out with an Ecochemie Autolab PGSTAT12 system (Utrecht, The Netherlands) employing a three-compartment cell with a working gold electrode and a platinum wire as counter electrode. All potentials were reported with respect to a Ag/AgCl reference electrode. All solutions were deaerated with nitrogen gas before use, keeping the gas flow over the solutions during experiments.

FT-IR measurements were performed employing a Bruker IFS66v spectrometer. All the spectra were obtained from 7000 to 550 cm^{-1} using a 4 cm^{-1} resolution. 250 scans were recorded for each spectrum and background was subtracted in all the cases. FT-IR measurements were carried out from KBr pellets.

Atomic Force Microscopy (AFM) data were obtained with a Nanoscope IIIa equipment (Veeco) under ambient conditions by using silicon tips, with a nominal spring constant in the 1–5 N/m range and a nominal tip radius of 8 nm (Bruker). Images have been taken in the intermittent contact mode.

2.3. Procedures

2.3.1. Preparation of the electrochemical biosensing platforms

Prior to each experiment, gold electrodes were polished with 1 μm diamond paste (Buehler) and rinsed with water. Then, they were conditioned to obtain a proper baseline and stable response by holding the potential at +2.0 V (vs Ag/AgCl) for 5 s in 0.1 M H_2SO_4 and then at −0.35 V (vs Ag/AgCl) for 10 s, followed by potential cycling from −0.20 to +1.5 V (vs Ag/AgCl) at 5 V/s for 2 min. Subsequently, the cyclic voltammogram characteristic of a clean polycrystalline gold electrode was recorded, from −0.2 to +1.5 V (vs Ag/AgCl), at 100 mV s^{-1}. The electrode was subsequently rinsed with water, air-dried and modified with 5 μL of the DNPs suspension (system denoted as DNPs/Au). Finally, 5 μL of the GOx or LOx stock solution was placed onto the DNPs/Au electrode surface (GOx/DNPs/Au or LOx/DNPs/Au). For control experiments, LOx/Au and GOx/Au platforms were also developed by placing 5 μL of the enzyme stock solution onto a bare Au electrode surface.

2.3.2. Samples for AFM measurements

Samples for determining the average diameter of diamond nanoparticles were prepared in a particular way due to the great tendency of DNPs to agglomerate [19]. It is necessary to deposit single nanoparticles on a flat substrate, such as silicon (surface roughness: 0.2 nm), in order to obtain their height distribution unambiguously. Silicon substrates were located at the bottom of a vase containing the suspension of DNPs in water and sonicated during one hour. In this way, the aggregates, thanks to the shaking process, were able to disaggregate to some extent [20], leading to deposits on the substrate with both aggregates and isolated DNPs. Afterwards, the DNPs modified surface was dried under nitrogen and measured by AFM in the intermittent contact mode. Note that to avoid tip convolution effects, the size distribution was obtained by measuring the height of the isolated DNPs.

2.3.3. Determination of L-lactic acid in real samples

The concentration of L-lactic acid in a white wine (purchased in a local market) was determined by the standard addition method. For this, 2.0 mL of wine sample, after dilution 1:100 in distilled water, were mixed with increasing volumes (0, 50, 100, 150, 200 and 250 μL) of a 0.010 M lactic acid standard solution and diluted to 10.0 mL in a volumetric flask with 0.1 M phosphate buffer (pH = 7.0) containing HMF (final concentration of HMF 1.0 mM). The L-lactic acid concentration obtained employing the developed biosensor was compared to those obtained by a commercial enzymatic assay kit according to the manufacturer's instructions. This enzymatic assay is based on L-lactate dehydrogenase and D-glutamate-pyruvate transaminase. The NADH formed was measured by the increase in absorbance at 340 nm and correlated with the L-lactic acid concentration.

3. Results and discussion

Diamond nanoparticles are available from different commercial sources. Depending on the specific synthesis conditions and purification procedures employed in their fabrication, the resulting nanomaterials can present different sizes and physicochemical properties and, therefore, differences in their surface chemistry [14], which clearly affect their subsequent behavior. In particular, previous studies have shown that DNPs diameter has a great influence on their reactivity [17,21]. Thereby, the percentage of the number of atoms on the DNPs surface, the number of functionality groups and the sp^2/sp^3 carbon ratio are

parameters greatly dependent on the size. As the DNPs size decreases, their properties become mainly determined by their surface [27]. When DNPs are employed for modifying electrodes, other factors, such as the nature of the underlying electrode, the immobilization method employed and the working conditions are also involved in the behavior of the resulting device.

In order to deepen our understanding of the influence of DNPs properties on electrocatalytic processes, we have nanostructured gold electrodes with diamond nanoparticles of 4 nm of nominal diameter (DNPs4) and subsequently we have modified it with lactate oxidase (or glucose oxidase, in some cases, in order to establish comparisons). The response of the LOx/DNPs4/Au system to lactate was studied by cyclic voltammetry (CV) and compared with the response of a LOx/DNPs9/Au biosensor.

3.1. Determination of the DNPs diameter histogram

So far, we have been referring to the nominal diameter of the DNPs provided by the supplier. At this stage, we are going to obtain the diameter distribution of the DNPs and its corresponding average value. For this purpose, we have registered several AFM images of a flat surface modified with DNPs4 (see Experimental section). Analyzing the height of more than 270 nanoparticles scattered over the surface (Fig. S1), we obtained an average height (diameter) value of $<h> = 3.7 \pm 1.5$ nm.

3.2. Response towards lactate of LOx/DNPs4/Au

Fig. 1A depicts the CV response for LOx/DNPs4/Au in the absence and in the presence of 0.5 mM of lactate in 0.1 M pH 7.0 phosphate buffer solution containing 1.0 mM HMF. In the absence of lactate (Fig. 1A, curve a), the cyclic voltammogram shows the typical redox response of the HMF(Fe^{II})/HMF(Fe^{III}) process in aqueous media at a formal potential of +0.30 V (vs Ag/AgCl) and a well-defined, but irreversible, peak close to the first one, at a potential value of +0.15 V (vs Ag/AgCl). This last peak only appears for systems containing simultaneously HMF and DNPs. Therefore, it is neither related with HMF nor DNP themselves, but rather with processes involving HMF on DNP surface.

Upon addition of lactate, two catalytic waves centered at +0.15 V and +0.30 V (vs Ag/AgCl) are observed (Fig. 1A, curve b). It is worth noting that this is the first time that we observe such simultaneous catalytic effect in similar systems (including redox enzymes and nanomaterials) [23–26], which in the first instance can be attributed to the presence of diamond nanoparticles. Nevertheless, not all types of DNPs promote this simultaneous catalytic effect, since it seems to depend on their size. To highlight this fact, in Fig. 1B the electrochemical response of the LOx/DNPs9/Au system is also displayed. Firstly, it should be noted that the peak at +0.15 V (vs Ag/AgCl) is not clearly observed (Fig. 1B, curve a). Secondly, upon addition of lactate a single catalytic wave centered at +0.30 V (vs Ag/AgCl) is obtained (Fig. 1B, curve b).

3.3. Electrochemical characterization of DNPs4 modified gold electrodes

In order to understand the unexpected behavior of the LOx/DNPs4/Au system, we have investigated the nature of peaks at +0.30 V (main peak) and +0.15 V (pre-peak) (vs Ag/AgCl), by obtaining cyclic voltammograms for DNPs4/Au electrode in 0.1 M pH 7.0 phosphate buffer solution containing HMF 1.0 mM at different scan rates. As can be observed in Fig. 2, the behavior of the pre-peak can be summarized as follows: i) its current intensity increases as the scan rate increases, but it becomes less well defined, ii) for scan rates equal or higher than 100 mV s^{-1}, it becomes a shoulder of the main peak, until it finally disappears for even higher scan rates.

Plots of anodic current intensity, corresponding to the main peak and the pre-peak, versus both scan rate and square root of scan rate were performed in order to determine which of them resulted in a straight line. It should be noted that these plots were made for scan rates from 10 to 100 mV s^{-1} since, as mentioned above, for higher scan rates the pre-peak is not enough well defined to measure its peak current. The plot of the anodic current intensity of the main peak versus square root of scan rate resulted in a straight line (inset A of Fig. 2) whereas versus scan rate gives a curved line (data not shown), indicating that the redox process was controlled by diffusion. Conversely, for the pre-peak, anodic current intensity versus scan rate resulted in a straight line (inset B of Fig. 2), suggesting an adsorption controlled process. Thus, HMF is partially bonded to the DNP surface. This result agrees well with previous studies, where infrared experiments confirmed the strong electrostatic affinity of the oxidized form of HMF for negatively charged diamond nanoparticles surfaces [17]. The negative charge of commercial DNP powders arises from acid cleaning steps that leave oxygen groups on the surface, particularly carboxyl groups [21–22]. According to data provided by the diamond nanoparticle supplier, DNPs4 and DNPs9 employed in the present work have —OH, —CN, —COOH, C—O—C and C═O functional groups on their surface, whose presence has been confirmed by IR measurements. The vibrational spectra of DNPs4 and DNPs9 (Fig. S2), show several bands associated to oxygen-containing surface groups such as ≡C—O—C≡, O—H and C═O (features at 1000–1150, 1620 and 3420, and 1386 cm^{-1} respectively) [21].

As concluded from the scan rate study, the pre-peak is associated to a surface confined process, in which HMF is adsorbed onto the DNP surface. Thus, working conditions can strongly influence the pre-peak behavior. Firstly, we have studied the effect of pH on the cyclic voltammetric response of HMF at a DNPs4/Au electrode. Concerning the main process at +0.30 V (vs Ag/AgCl), it was found that both potential and current values of the cathodic and anodic peaks remain constant with pH, as it was expected for oxidation/reduction of HMF since H^+ ions are not involved in the process. However, pH value plays a key role in the case of the pre-peak. HMF is a neutral compound at its reduced form and a positively charged compound at its oxidized form. For pHs higher than 6.0, the pre-peak is clearly observed suggesting that, at these working conditions, DNPs surface functional groups

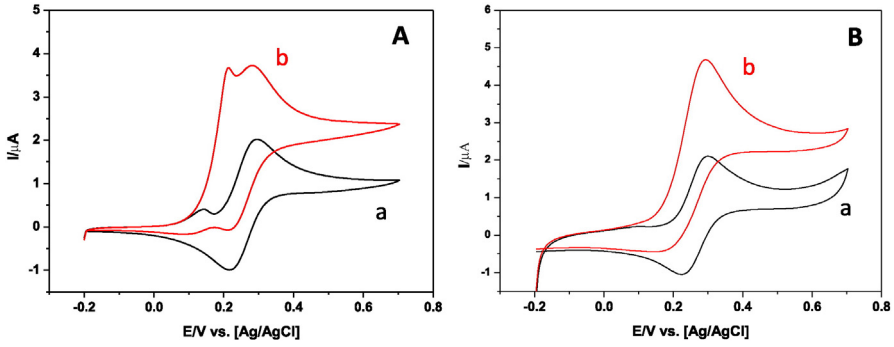

Fig. 1. Cyclic voltammetric response for (A) LOx/DNPs4/Au and (B) LOx/DNPs9/Au biosensors in contact with a 0.1 M phosphate buffer solution (pH 7.0) containing 1.0 mM HMF in absence (curves a) and in presence of 0.5 mM of lactate (curves b). Scan rate v = 0.01 V/s.

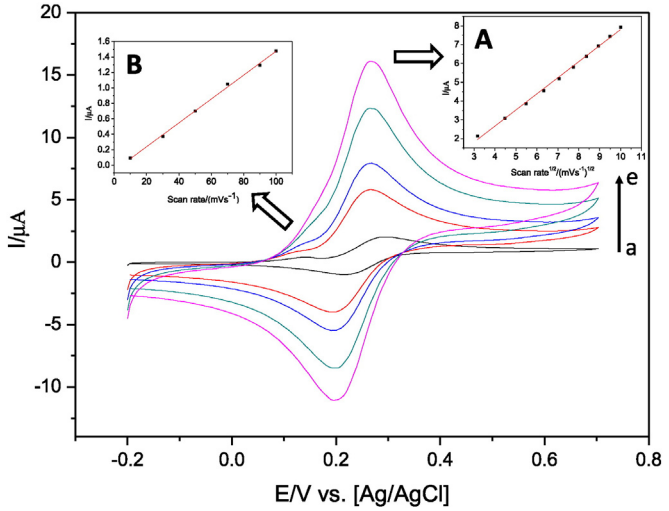

Fig. 2. Cyclic voltammograms of 1.0 mM HMF in 0.1 M phosphate buffer solution (pH 7) at a DNPs4/Au electrode at different scan rates: (a) 10 mV s^{-1}, (b) 50 mV s^{-1}, (c) 90 mV s^{-1}, (d) 100 mV s^{-1} and (e) 200 mV s^{-1}. Inset A: Plot of anodic current intensity at +0.30 V vs square root of scan rate. Inset B: Plot of anodic current intensity at +0.15 V vs scan rate.

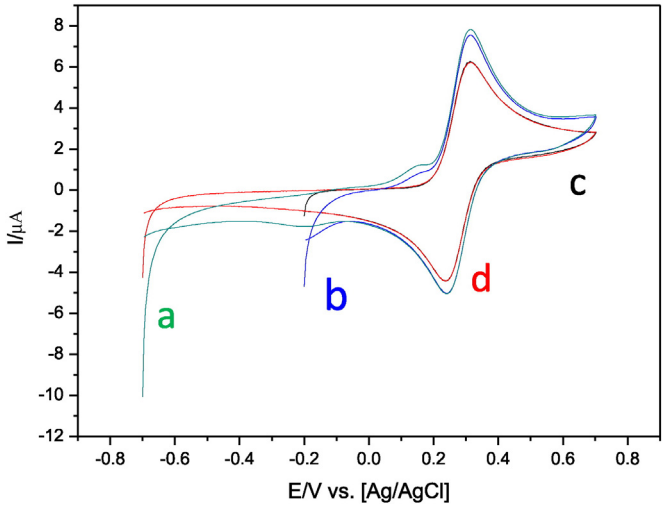

Fig. 4. Cyclic voltammetric response for DNPs4/Au system in contact with 1.0 mM HMF in 0.1 M phosphate buffer solution (pH = 7.0) in the potential range from −0.7 V to +0.7 V (curve a) and from −0.2 V to +0.7 V (vs Ag/AgCl) (curve b). Curves (c) and (d) correspond to CV response from −0.2 V to +0.7 V and from −0.7 V to +0.7 V (vs Ag/AgCl), respectively, for an unmodified Au electrode. Scan rate v = 0.1 V/s.

(such as carboxylic acids) are probably deprotonated and therefore adsorption of HMF is enhanced. For pHs lower than 6.0, adsorption of HMF over a DNP surface (where carboxylic acids are probably protonated) is not promoted, as suggested by the absence of the pre-peak. These results can be clearly observed in Fig. 3, where cyclic voltammograms for DNPs4/Au system in 0.1 M phosphate buffer solution containing HMF 1.0 mM at pH 4.5 (curve a) and pH 7.0 (curve b) are compared.

Secondly, we have recorded the cyclic voltammetric response of HMF at both a DNPs4/Au electrode (Fig. 4, curves a, b) and a bare gold electrode (Fig. 4, curves c, d), starting at two different initial potential values (E_i = −0.7 V and −0.2 V (vs Ag/AgCl)). As can be observed in Fig. 4, the modification of a gold electrode with DNPs4 enhances the electrochemical response of the redox compound in solution, HMF, with respect to the unmodified electrode. This enhancement is a consequence of the following catalytic feedback mechanism [17,18]: after oxidation of HMF(Fe^{II}) to HMF(Fe^{III}) over the electrode surface, an electron transfer from DNPs to HMF(Fe^{III}) occurs, allowing a rapid regeneration of HMF(Fe^{II}) and enhancing oxidation currents. Accordingly, enhancements of reduction currents are produced when HMF(Fe^{II}), obtained from reduction of HMF(Fe^{III}) over the electrode, gives an electron to DNPs, regenerating HMF(Fe^{III}). This behavior can be related to the ability of DNPs to act as both source and sink of electrons, which has as origin the overlapping of molecular orbitals of functionalities such as C═C and C═O, leading to electronic states (π and π*) with energy values lying within the diamond band gap [13,14]. In principle, the extent of the enhancement depends on the surface density of these functionalities [17]. Furthermore, it should be taken into account that usually a finite amount of sp^2 bonding on diamond nanoparticles coexists with sp^3 ones, providing electronic conductivity. The presence of these sp^2 bonding at particle surfaces has been shown by neutron diffraction measurements [20,21,27–29].

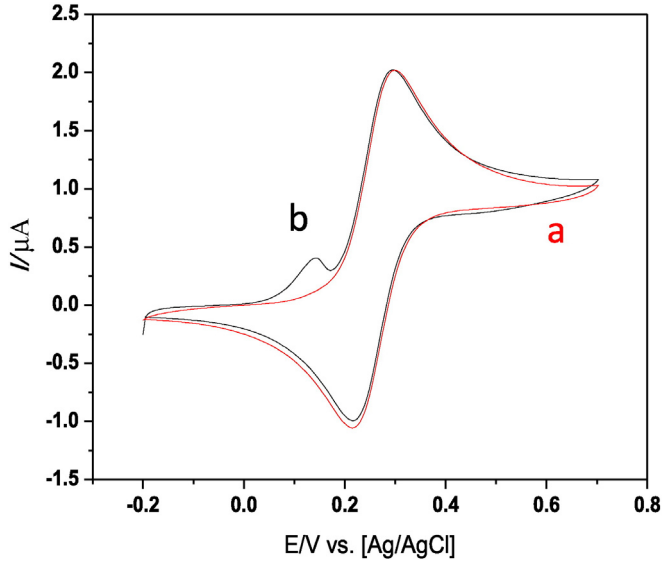

Fig. 3. Cyclic voltammetric response for DNPs4/Au system in contact with 1.0 mM HMF in 0.1 M phosphate buffer solution at (a) pH = 4.5 and (b) pH = 7.0. Scan rate v = 0.01 V/s.

The enhancement of the electrochemical response of HMF at a DNPs modified electrode is slightly dependent on the applied initial potential (E_i). A more cathodic E_i leads to higher enhancement currents of the pre-peak and the main peak. This behavior seems to indicate an increase of the DNPs capacity to donate electrons that could be a consequence of the initial reduction of DNPs at −0.7 V (vs Ag/AgCl). Reduction at the electrode allows filling available surface states with electrons, enhancing DNPs capability as source of electrons and increasing therefore the extent of the feedback mechanism. The influence of cathodic and anodic pretreatments on the surface activity of diamond films have been studied by several research groups [30–33]. Moreover, concerning the pre-peak, it seems that adsorption of HMF onto DNPs surface is also improved when cyclic voltammetry is started at more cathodic potential, −0.7 V towards −0.2 V (vs Ag/AgCl), since in this case a more intense wave at +0.15 V (vs Ag/AgCl) is observed (by comparing curves a and b in Fig. 4).

Finally, a large initial reduction current is observed for electrodes modified with DNPs (Fig. 4, curves a, b), which is smaller or even absent for unmodified electrodes (Fig. 4, curves c, d). In principle, taking into account that there are not reducible compounds in solution, this reduction current at the start of the CV could be assigned to spontaneous generation of HMF(Fe^{III}) at the DNPs surface. However, this explanation is discarded because a current reduction is also present in cyclic voltammograms recorded employing the same DNPs modified electrode (DNPs/Au) in phosphate buffer solution without HMF. Additionally, since experiments were performed in deaerated media, the initial current reduction cannot be attributed to oxygen catalysis phenomena caused by the presence of DNPs. Then, it can be probably related to the own reduction of DNPs at the gold electrode.

3.4. Electrochemical characterization of LOx modified DNPs/Au electrodes

It has been reported that DNPs are able to promote direct electron transfer (DET) between an enzyme and the underlying electrode [16]. However, the cyclic voltammetric response of the LOx/DNPs4/Au system in PBS 0.1 M (pH = 7.0) is featureless (Fig. 5, curve a). In contrast, the cyclic voltammogram corresponding to LOx/DNPs9/Au (Fig. 5, curve b) shows a reversible wave at −0.4 V (vs Ag/AgCl), which is consistent with the reversible oxidation-reduction of the FAD/$FADH_2$ of the enzyme according to:

$$LOx(FAD) + 2e^- + 2H^+ \leftrightarrow LOx(FADH_2) \quad (1)$$

After 100 scans, the redox peak at −0.4 V (vs Ag/AgCl) diminishes around 8% (data not shown), demonstrating that DET remains over continuously cycling.

Control experiments carried out employing a bare gold, a DNPs/Au and a LOx/Au electrodes yielded featureless voltammograms (data not shown), demonstrating that DNPs9 are able to promote DET between redox enzymes and the underlying electrodes.

The cyclic voltammetric response obtained by employing a different enzyme was obtained in order to assess whether the mentioned behavior is specific for LOx. Results obtained for glucose oxidase (GOx), displayed in Fig. S3, confirm that peaks corresponding to FAD/$FADH_2$ are observed no matter the oxidoreductase employed, but only for DNPs9. Therefore, it seems that DET between DNPs and enzymes is not promoted in all cases. In this sense, the relative orientation of the enzyme redox active site and the DNPs can be different depending on the DNP size. For example, LOx (or GOx) and DNPs9 have a similar size, leading to an adequate accommodation of the enzyme onto the nanomaterial. Conversely, DNPs4 is smaller than the enzyme, forcing a different positioning.

3.5. Biosensor response. Analytical properties

The response of the LOx/DNPs4/Au developed biosensor towards increasing concentrations of lactate is studied (Fig. 6A).

According to the following catalytic mechanism, upon addition of lactate, LOx catalyzes the oxidation of lactate to pyruvate (Eq. (2)), while the electrons are transferred to $(HMF)_{ox}$, regenerating the enzyme activity (Eq. (3)). The re-oxidation of HMF (Eq. (4)) leads to a response (curves b–f), which is proportional to the amount of lactate present in the solution.

$$\text{L-lactate} + (LOx)_{ox} \rightarrow \text{Pyruvate} + (LOx)_{red} \quad (2)$$

$$(LOx)_{red} + (HMF)_{ox} \rightarrow (LOx)_{ox} + (HMF)_{red} \quad (3)$$

$$(HMF)_{red} - e^- \rightarrow (HMF)_{ox} \quad (4)$$

Since HMF molecules involved in this catalytic process can be both in solution and adsorbed onto the DNPs surface, two catalytic waves at +0.30 V and +0.15 V (vs Ag/AgCl) are obtained. The analytical properties (linear concentration range, sensitivity and detection limit) of the developed biosensing platform can be obtained from both catalytic waves. However, comparison of calibration plots obtained by measuring the catalytic current at +0.15 V (Fig. 6B) or at +0.30 V (vs Ag/AgCl) (data not shown) show that better linear concentration range and sensitivity are obtained for the first case. As can be observed in the inset of Fig. 6B, the calibration plot was linear from 0.02 mM to 1.2 mM, with the following equation: I (μA) = 0.107 + 6.1 C (mM) (R^2 = 0.998). The sensitivity, calculated from the slope of the plot, was of 6.1 μA mM^{-1}. The detection limit, calculated as the ratio between three times the standard deviation of background current and the sensitivity, was 5.3 μM. Concerning the calibration plot measured at +0.30 V (vs Ag/AgCl) a linear concentration range from 0.03 mM to 0.55 mM, a sensitivity of 3.6 μA mM^{-1} and a detection limit of 9.1 μM are obtained. Finally, the stability of biosensors was also evaluated. Firstly, we have obtained the biosensor response to 0.4 mM of lactate 50 times in order to assess the repeatability, obtaining a RSD value of 1%. Secondly, we have obtained the biosensor response to 0.4 mM of lactate after 30 days of storage at 4 °C. Under these conditions, biosensors retain 98% of their initial response whereas the system without DNPs retains only the 50%.

Storage stability data allow deriving several conclusions regarding the role of DNPs in enzyme adsorption. The better storage stability obtained for the LOx/DNPs4/Au system compared with the LOx/Au system indicate that in the absence of DNPs the enzyme is more easily released from the transducer and/or the enzymatic activity is lost more rapidly. These data suggest that DNPs lead to a stronger enzyme adsorption which hampers its release from the surface and/or provides a more adequate microenvironment for the enzyme conformational stabilization that preserves the enzymatic activity. Moreover, the presence of DNPs can induce a different positioning of the enzyme onto their surface compared with that on a bare gold surface as has been concluded from the results presented above concerning DNPs direct electron transfer promotion.

The analytical response, specially that measured at +0.15 V (vs Ag/AgCl), compares well with those obtained for other lactate-based biosensors developed in our laboratory that also include nanomaterials and employ HMF as redox mediator [18,24–26]. Here, it is important to point out that the LOx/DNPs4/Au biosensor developed in the present work presents an important advantage related to the lower potential required for lactate detection (+0.15 V towards +0.30 V (vs Ag/AgCl), which represents 150 mV), which minimizes the potential interferences. In this sense, we have obtained the LOx/DNPs4/Au biosensor response to 0.7 mM of lactate in absence and presence of acetaminophen (0.1 mM), ascorbic acid (0.1 mM) and uric acid (0.1 mM), demonstrating that these potential interferences have negligible effect.

3.6. Determination of L-lactic acid in real samples

We have applied the LOx/DNPs4/Au biosensor for lactic acid determination in wine. The results obtained, following the procedure described in the experimental section, were compared with those obtained employing a commercial enzymatic assay kit. The average value obtained for 3 measurements using different biosensors

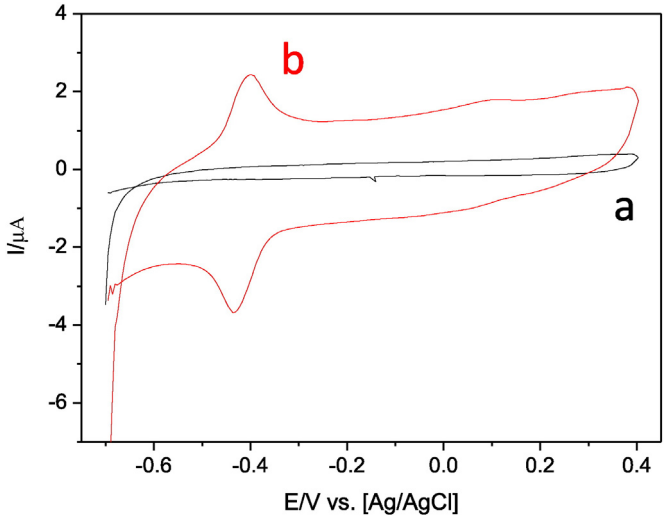

Fig. 5. Cyclic voltammetric response for LOx/DNPs4/Au (curve a) and LOx/DNPs9/Au (curve b) in contact with 0.1 M phosphate buffer solution (pH = 7.0) in the absence of substrate. Scan rate v = 0.1 V/s.

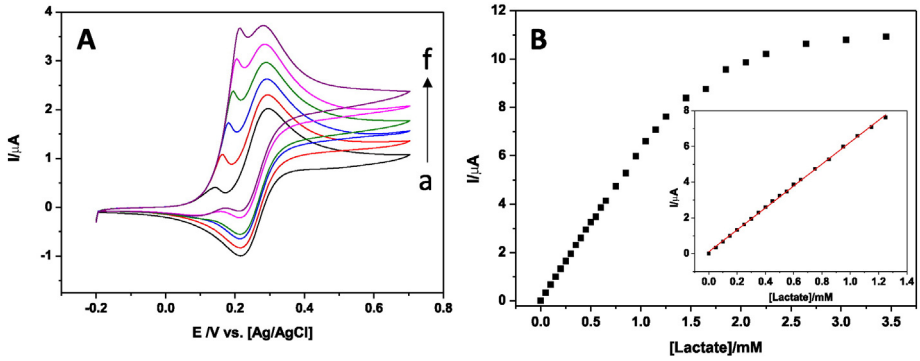

Fig. 6. (A) Cyclic voltammetric response for LOx/DNPs4/Au biosensor in contact with 1.0 mM HMF in 0.1 M phosphate buffer solution (pH = 7.0) in absence (curve a) and in presence of 0.1 mM, 0.2 mM, 0.3 mM, 0.4 mM and 0.5 mM of lactate (curves b–f). Scan rate v = 0.01 V/s. (B) Calibration curve obtained from cyclic voltammograms, measuring the current intensity at +0.15 V (vs Ag/AgCl). The inset shows the linear concentration range.

(14.6 ± 0.9 mM) agrees well with those obtained by the enzymatic kit (14.6 ± 0.7 mM). However, the employment of the biosensor method is more rapid, direct and economical.

4. Conclusions

DNPs4 immobilized onto gold electrodes (DNPs4/Au) cause the appearance of an oxidation pre-peak at +0.15 V (vs Ag/AgCl) for pH > 6 and low scan rates, accompanying the typical ferrocene (Fe^{II})/ferrocenium (Fe^{III}) peak at +0.30 V (vs Ag/AgCl). The pre-peak current intensity shows a linear dependence with scan rate, suggesting an adsorption controlled process. Conversely, the peak current of the main process at +0.30 V (vs Ag/AgCl) shows a linear dependence with square root of scan rate, indicating a redox process controlled by diffusion. The response of LOx/DNPs4/Au biosensor to lactate shows two simultaneous bioelectrocatalytic processes at +0.15 V and +0.30 V (vs Ag/AgCl), indicating that different feedback mechanisms (through both HMF adsorbed onto DNPs and HMF in solution) are taking place. The possibility to measure the biosensor response to lactate at a potential value of +0.15 V (vs Ag/AgCl) is very convenient, from the point of view of avoiding potential interferences. The resulting LOx/DNPs4/Au biosensor shows a linear concentration range from 0.02 mM to 1.2 mM, a sensitivity of 6.1 μA mM^{-1} and a detection limit of 5.3 μM, as well as an excellent stability. The developed biosensor has been applied to lactate determination in wine samples, demonstrating its suitability to measure this analyte in a complex matrix. Finally, although DNPs4 do not promote the direct electron transfer between the enzyme and the underlying electrode, DNPs9 do it, supporting the idea that different sizes and physicochemical properties of DNPs affect their resulting surface chemistry.

Supplementary data to this article can be found online at http://dx.doi.org/10.1016/j.bioelechem.2016.05.007.

Acknowledgments

This work has been supported by Ministerio de Economía y Competitividad (Project nos. CTQ2014-53334-C2-1-R, FIS2012-38866-C05-05 and CTQ2015-71955-REDT) and Comunidad Autónoma de Madrid (Project NANOAVANSENS S2013/MIT-3029). We want to give thanks to Pascual Torres and Luis Larumbe from FTIR Laboratory of SIdI (UAM) by spectroscopic measurements.

References

[1] Z. Wang, Z. Dai, Carbon nanomaterial-based electrochemical biosensors: an overview, Nanoscale 7 (2015) 6420–6431.
[2] J. Wang, Electrochemical biosensing based on noble metal nanoparticles, Microchim. Acta 177 (2012) 245–270.
[3] S. Guo, S. Dong, Graphene nanosheet: synthesis, molecular engineering, thin film, hybrids, and energy and analytical applications, Chem. Soc. Rev. 40 (2011) 2644–2672.
[4] A.M. Schrand, S.A. Ciftan Hens, O.A. Shenderova, Nanodiamond particles: properties and perspectives for bioapplications, Crit. Rev. Solid State 34 (2009) 18–74.
[5] H.B. Man, D. Ho, Diamond as a nanomedical agent for versatile applications in drug delivery, imaging, and sensing, Phys. Status Solidi A 209 (2012) 1609–1618.
[6] A. Krueger, New carbon materials: biological applications of functionalized nanodiamond materials, Chem. Eur. J. 14 (2008) 1382–1390.
[7] V.N. Mochalin, O. Shenderova, D. Ho, Y. Gogotsi, The properties and applications of nanodiamonds, Nat. Nanotechnol. 7 (2012) 11–23.
[8] C. Gaillard, H.A. Girard, C. Falck, V. Paget, V. Simic, N. Ugolin, P. Bergonzo, S. Chevillard, J.C. Arnault, Peptide nucleic acid-nanodiamonds: covalent and stable conjugates for DNA targeting, RSC Adv. 4 (2014) 3566–3572.
[9] W. Zhang, K. Patel, A. Schexnider, S. Banu, A.D. Radadia, Nanostructuring of biosensing electrodes with nanodiamonds for antibody immobilization, ACS Nano 8 (2014) 1419–1428.
[10] W. Zhao, J.-J. Xu, Q.-Q. Qiu, H.-Y. Chen, Nanocrystalline diamond modified gold electrode for glucose biosensing, Biosens. Bioelectron. 22 (2006) 649–655.
[11] E. Nicolau, J. Méndez, J.J. Fonseca, K. Griebenow, C.R. Cabrera, Bioelectrochemistry of non-covalent immobilized alcohol dehydrogenase on oxidized diamond nanoparticles, Bioelectrochemistry 85 (2012) 1–6.
[12] C.D. Clark, P.J. Dean, P.V. Harris, Intrinsic edge absorption in diamond, P. Roy. Soc. A - Math. Phy. 277 (1964) 312–329.
[13] K.B. Holt, D.J. Caruana, E.J. Millán-Barrios, Electrochemistry of undoped diamond nanoparticles: accessing surface redox states, J. Am. Chem. Soc. 131 (2009) 11272–11273.
[14] K.B. Holt, Undoped diamond nanoparticles: origins of surface redox chemistry, Phys. Chem. Chem. Phys. 12 (2010) 2048–2058.
[15] J. Scholz, A.J. McQuillan, K.B. Holt, Redox transformations at nanodiamond surfaces revealed by in situ infrared spectroscopy, Chem. Commun. 47 (2011) 12140–12142.
[16] J.-T. Zhu, C.-G. Shi, J.-J. Xu, H.-Y. Chen, Direct electrochemistry and electrocatalysis of hemoglobin on undoped nanocrystalline diamond modified glassy carbon electrode, Bioelectrochemistry 71 (2007) 243–248.
[17] T.S. Varley, M. Hirani, G. Harrison, K.B. Holt, Nanodiamond surface redox chemistry: influence of physicochemical properties on catalytic processes, Faraday Discuss. 172 (2014) 349–364.
[18] M. Briones, E. Casero, M.D. Petit-Domínguez, M.A. Ruiz, A.M. Parra-Alfambra, F. Pariente, E. Lorenzo, L. Vázquez, Diamond nanoparticles based biosensors for efficient glucose and lactate determination, Biosens. Bioelectron. 68 (2015) 521–528.
[19] I.I. Kulakova, Surface chemistry of nanodiamonds, Phys. Solid State 46 (2004) 636–643.
[20] A. Krüger, F. Kataoka, M. Ozawa, T. Fujino, Y. Suzuki, A.E. Aleksenskii, A. Ya. Vul', E. Osawa, Unusually tight aggregation in detonation nanodiamond: identification and disintegration, Carbon 43 (2005) 1722–1730.
[21] O.A. Williams, J. Hees, C. Dieker, W. Jäger, L. Kirste, C.E. Nebel, Size-dependent reactivity of diamond nanoparticles, ACS Nano 4 (2010) 4824–4830.
[22] H.P. Boehm, Surface oxides on carbon and their analysis: a critical assessment, Carbon 40 (2002) 145–149.
[23] M. Barbadillo, E. Casero, M.D. Petit-Domínguez, L. Vázquez, F. Pariente, E. Lorenzo, Gold nanoparticles-induced enhancement of the analytical response of an electrochemical biosensor based on an organic-inorganic hybrid composite material, Talanta 80 (2009) 797–802.
[24] E. Casero, C. Alonso, L. Vázquez, M.D. Petit-Domínguez, A.M. Parra-Alfambra, M. de la Fuente, P. Merino, S. Álvarez-García, A. de Andrés, F. Pariente, E. Lorenzo, Comparative response of biosensing platforms based on synthesized graphene oxide and electrochemically reduced graphene, Electroanalysis 25 (2013) 154–165.
[25] E. Casero, C. Alonso, M.D. Petit-Domínguez, L. Vázquez, A.M. Parra-Alfambra, P. Merino, S. Álvarez-García, A. de Andrés, E. Suárez, F. Pariente, E. Lorenzo, Lactate biosensor based on a bionanocomposite composed of titanium oxide nanoparticles, photocatalytically reduced graphene, and lactate oxidase, Microchim. Acta 181 (2014) 79–87.
[26] A.M. Parra-Alfambra, E. Casero, M.D. Petit-Domínguez, M. Barbadillo, F. Pariente, L. Vázquez, E. Lorenzo, New nanostructured electrochemical biosensors based on

three-dimensional (3-mercaptopropyl)-trimethoxysilane network, Analyst 136 (2011) 340–347.
[27] S. Osswald, G. Yushin, V. Mochalin, S.O. Kucheyev, Y. Gogotsi, Control of sp^2/sp^3 carbon ratio and surface chemistry of nanodiamond powders by selective oxidation in air, J. Am. Chem. Soc. 128 (2006) 11635–11642.
[28] A.S. Barnard, M. Sternberg, Crystallinity and surface electrostatics of diamond nanocrystals, J. Mater. Chem. 17 (2007) 4811–4819.
[29] B. Palosz, C. Pantea, E. Grzanka, S. Stelmakh, T. Proffen, T.W. Zerda, W. Palosz, Investigation of relaxation of nanodiamond surface in real and reciprocal spaces, Diam. Relat. Mater. 15 (2006) 1813–1817.
[30] T.N. Rao, D.A. Tryk, K. Hashimoto, A. Fujishima, Band-edge movements of semiconducting diamond in aqueous electrolyte induced by anodic surface treatment, J. Electrochem. Soc. 146 (1999) 680–684.
[31] H. Notsu, I. Yagi, T. Tatsuma, D.A. Tryk, A. Fujishima, Surface carbonyl groups on oxidized diamond electrodes, J. Electroanal. Chem. 492 (2000) 31–37.
[32] H. Notsu, I. Yagi, T. Tatsuma, D.A. Tryk, A. Fujishima, Introduction of oxygen-containing functional groups onto diamond electrode surfaces by oxygen plasma and anodic polarization, Electrochem. Solid-St. Letters 2 (1999) 522–524.
[33] Y. Jiang, D. Liu, Z. Jiang, B. Mao, X. Ma, Q. Li, Investigation on electrochemically cathodic polarization of boron-doped diamond electrodes and its influence on lead ions analysis, J. Electrochem. Soc. 161 (2014) H410–H415.